


Geodesic structure of the Euler-Heisenberg static black hole

Daniel Amaro ^{*}

*Departamento de Física, Universidad Autónoma Metropolitana-Iztapalapa,
Apdo. Postal 55–534, C.P. 09340, Ciudad de México, México*

Alfredo Macías [†]

*Physics Department, Universidad Autónoma Metropolitana-Iztapalapa,
PO. Box 55–534, C.P. 09340, CDMX, México*

 (Received 16 August 2020; accepted 28 October 2020; published 19 November 2020)

We derive an electrically charged static black hole spacetime of the Einstein-Euler-Heisenberg theory, in terms of the Plebański dual variables. This solution is a nonlinear electromagnetic generalization of the Reissner-Nordström solution, and it is characterized by the mass M , the electric charge Q of the black hole, and the Euler-Heisenberg nonlinear constant, which includes the fine structure constant α . We study all possible equatorial trajectories of test particles. Moreover, the orbits of photons are analyzed by means of the effective Plebański pseudometric related to the geometrical metric and to the electromagnetic energy-momentum tensor. The shape of the shadow of the black hole is also presented and discussed.

DOI: [10.1103/PhysRevD.102.104054](https://doi.org/10.1103/PhysRevD.102.104054)

I. INTRODUCTION

The coupling of the Einstein theory to the class of nonlinear electrodynamics (NLED) proposed by Plebański [1] admits regular black hole solutions [2], i.e., black holes whose curvature invariants R , $R_{\mu\nu}R^{\mu\nu}$, and $R_{\mu\nu\alpha\beta}R^{\mu\nu\alpha\beta}$ are nonsingular. Therefore, there exist nowadays a great revival of interest on it.

The interest in nonlinear electrodynamics began in 1912 when Mie [3] put forward the first model for nonlinear electrodynamics. Between 1932 and 1935 Born and Infeld [4] proposed their nonlinear theory, which represents a classical generalization of the Maxwell-Lorentz theory for accommodating stable solutions for the description of electrons. Because of the nonlinearity of the electromagnetic theory, the field of a point charge turns out to be finite at $r = 0$, in contrast to the well-known $1/r^2$ singularity of the Coulomb field in Maxwell-Lorentz electrodynamics. Moreover, the characteristic surface, the light cone, depends on the field strength, and the superposition principle for the electromagnetic field does not hold any longer.

Black hole solutions to the Born-Infeld (BI) nonlinear electrodynamics have been found first by Hoffmann [5] in 1935 and later by Salazar *et al.* [6] in 1987. Then, Plebański [1] postulated a more general nonlinear electrodynamics, which contains the Born-Infeld theory as special case. Parity violating terms could emerge in Plebański nonlinear

electrodynamics [7]. A regular black hole solution to this theory has been obtained by Ayón-Beato *et al.* [2] in 1998.¹ Additionally, Bretón in 2002 [8] studied the trajectories of test particles in a geometry that is the Born-Infeld nonlinear electromagnetic generalization of the Reissner-Nordström solution.

Currently, there exists a revival of interest in nonlinear electrodynamics since the effective theory arising from superstrings is an electrodynamics of the Born-Infeld type [9–12]. Besides, much attention has been deserved to the interpretation of the solutions to the Born-Infeld equations as states of D-branes [13].

Moreover, quantum electrodynamic vacuum corrections to the Maxwell-Lorentz theory can be accounted for by an effective nonlinear theory derived by Euler and Heisenberg [14,15]. The vacuum is treated as a specific type of medium, the polarizability and magnetizability properties of which are determined by the clouds of virtual charges surrounding the real currents and charges [16]. Recently, Brodin *et al.* [17] proposed a possible direct measurement of the Euler-Heisenberg effect. This theory is a valid physical theory [18], and it is the low field limit of the Born-Infeld one [19].

On the other hand, the concepts of a black hole shadow surrounded by a photon ring have played an important role since they are crucial for the interpretation of the observations recently reported by the Event Horizon Telescope team from the supermassive black hole encountered at the

^{*}amaro@xanum.uam.mx
[†]amac@xanum.uam.mx

¹The curvature invariants mentioned above are nonsingular. We do not know if its geodesic completeness has been studied.

nucleus of the galaxy M87 [20]. The shadow at its center contains the event horizon, i.e., a spherical surface that represents a point of no return. Since light can cross the surface only one way, inwards, the sphere should look completely black. Close to the event horizon light rays bend so much that they effectively orbit the black hole, forming a photon ring [21].

In this paper, we rederive a static, spherically symmetric, electrically charged black hole solution, by means of the Plebański dual variables. This geometry is the Einstein-Euler-Heisenberg (EEH) nonlinear electromagnetic generalization of the Reissner-Nordström (RN) black hole solution, characterized by its charge Q , its mass M , and the Euler-Heisenberg constant, which includes the fine structure constant α . The effective potentials of all possible equatorial geodesics of test particles are studied. We consider neutral massive and massless particles, charged particles, and photons. Additionally, the shape of its shadow is analyzed.

It turns out that the nonlinearity of the electromagnetic field modifies the size of the horizon as well as the effective geometry seen by the Euler-Heisenberg nonlinear photons.

The outline of the paper is as follows: In Sec. II the Einstein-Euler-Heisenberg theory is revisited, and the dual variables are introduced. In Sec. III the static electrically charged black hole solution of the theory is derived; the event horizon is studied. Then, in Sec. IV, the effective potentials for all the possible equatorial trajectories of test particles are presented and analyzed. We consider uncharged massive and massless particles, charged particles and photons. In Sec. V the shape of the shadow of the electrically charged Einstein-Euler-Heisenberg black hole is obtained and discussed. In Sec. VI the conclusions and a summary of the work are presented.

II. THE EINSTEIN-EULER-HEISENBERG THEORY AND DUAL VARIABLES

We revisit in this section the basic features of nonlinear electrodynamics proposed by Euler and Heisenberg [14] in the formalism introduced by Plebański [1] for solutions of Petrov type-D.

The action for Einstein gravity minimally coupled to the Euler-Heisenberg theory reads [14,22]

$$S = \frac{1}{16\pi G} \int_{M_4} d^4x \sqrt{-g} R + \frac{1}{4\pi} \int_{M_4} d^4x \sqrt{-g} \left(-X + \frac{2\alpha^2}{45m^4} \{4X^2 + 7Y^2\} \right), \quad (1)$$

where R is the Ricci scalar curvature, G is the Newton's constant which we will take $G = 1$, m the electron mass, and α the fine structure constant, and the variables X and Y are the only two independent relativistic invariants constructed from the Maxwell field in four dimensions, which are defined as

$$X = \frac{1}{4} F_{\mu\nu} F^{\mu\nu}, \quad Y = \frac{1}{4} F_{\mu\nu} {}^*F^{\mu\nu}, \quad (2)$$

${}^*F_{\mu\nu}$ is the dual of the Faraday tensor $F_{\mu\nu} = A_{\mu;\nu} - A_{\nu;\mu}$, and it is defined as usual ${}^*F_{\mu\nu} = \frac{1}{2\sqrt{-g}} \epsilon_{\mu\nu\sigma\rho} F^{\sigma\rho}$, and $\epsilon_{\mu\nu\sigma\rho}$ is the completely antisymmetric tensor that satisfies $\epsilon_{\mu\nu\sigma\rho} \epsilon^{\mu\nu\sigma\rho} = -4!$.

The equations of motion derived from this action are more easily written in terms of the Legendre dual description of nonlinear electrodynamics [1], which involves the introduction of the tensor $P_{\mu\nu} = B_{\mu;\nu} - B_{\nu;\mu}$ defined by

$$dL(X, Y) = -\frac{1}{2} P^{\mu\nu} dF_{\mu\nu}, \quad (3)$$

where $L(X, Y)$ is the Lagrangian density for the Euler-Heisenberg nonlinear electrodynamics. Note that $P_{\mu\nu}$ coincides with $F_{\mu\nu}$ for the linear Maxwell theory. In general it reads

$$P_{\mu\nu} = -(L_X F_{\mu\nu} + L_Y {}^*F_{\mu\nu}), \quad (4)$$

where subscripts on L denote differentiation. In our case it reads

$$P_{\mu\nu} = F_{\mu\nu} - \frac{4\alpha^2}{45m^4} \{4X F_{\mu\nu} + 7Y {}^*F_{\mu\nu}\}. \quad (5)$$

The components of $P_{\mu\nu}$ are just the electric induction \mathbf{D} and the magnetic field \mathbf{H} ; therefore (5) are the constitutive relations of the Euler-Heisenberg nonlinear electrodynamics. We denote by s and t the two independent invariants in terms of the dual Plebański variables $P_{\mu\nu}$ defined in the following way:

$$s = -\frac{1}{4} P_{\mu\nu} P^{\mu\nu}, \quad t = -\frac{1}{4} P_{\mu\nu} {}^*P^{\mu\nu}, \quad (6)$$

where ${}^*P_{\mu\nu} = \frac{1}{2\sqrt{-g}} \epsilon_{\mu\nu\sigma\rho} P^{\sigma\rho}$.

The covariant Hamiltonian $H(s, t)$ is written as

$$H(s, t) = -\frac{1}{2} P^{\mu\nu} F_{\mu\nu} - L. \quad (7)$$

For the Euler-Heisenberg theory the Hamiltonian (up to terms of higher order in α) reads

$$H(s, t) = s - \frac{2\alpha^2}{45m^4} \{4s^2 + 7t^2\}. \quad (8)$$

The equations of the motion for the coupled system read [6]

$$D_\mu P^{\mu\nu} = 0, \quad R_{\mu\nu} - \frac{1}{2} R g_{\mu\nu} = 8\pi T_{\mu\nu}, \quad (9)$$

with the energy-momentum tensor,

$$T_{\mu\nu} = \frac{1}{4\pi} [H_s P_{\mu}^{\beta} P_{\nu\beta} + g_{\mu\nu} (2sH_s + tH_t - H)]. \quad (10)$$

The energy-momentum tensor for the Euler-Heisenberg nonlinear electromagnetic field is given by

$$T_{\mu\nu} = \frac{1}{4\pi} \left[\left(1 - \frac{16\alpha^2}{45m^4} s \right) P_{\mu}^{\beta} P_{\nu\beta} + g_{\mu\nu} \left(s - \frac{2\alpha^2}{45m^4} \{12s^2 + 7t^2\} \right) \right], \quad (11)$$

or in terms of the standard Maxwell variables,

$$T_{\mu\nu} = \frac{1}{4\pi} \left[\left(1 - \frac{16\alpha^2}{45m^4} X \right) F_{\mu}^{\beta} F_{\nu\beta} - \frac{28\alpha^2}{45m^4} Y (F_{\mu}^{\beta*} F_{\nu\beta} + {}^*F_{\mu}^{\beta} F_{\nu\beta}) - g_{\mu\nu} \left(X - \frac{2\alpha^2}{45m^4} \{4X^2 + 21Y^2\} \right) \right]. \quad (12)$$

Setting $\alpha = 0$, Eq. (12) reduces to the standard linear Maxwell energy-momentum tensor.

To obtain the original variables we use the constitutive or material equations that relate $F_{\mu\nu}$ with $P_{\mu\nu}$. These are

$$F_{\mu\nu} = [H_s + H_t] P_{\mu\nu} = \left(1 - \frac{4\alpha^2}{45m^4} \{4s + 7t\} \right) P_{\mu\nu}. \quad (13)$$

III. ELECTRICALLY CHARGED STATIC BLACK HOLE SOLUTIONS

In order to obtain the Einstein-Euler-Heisenberg generalization of the Reissner-Nordström solution, we consider the following static and spherically symmetric black hole metric:

$$ds^2 = -f(r)dt^2 + f(r)^{-1}dr^2 + r^2(d\theta^2 + \sin^2\theta d\phi^2), \quad (14)$$

with the signature $\{-, +, +, +\}$ and $f(r) = 1 - 2m(r)/r$, and look for electrically charged black hole solutions. It is important to mention the fact that, in the framework of nonlinear electrodynamics, if one is looking for an exact electrically charged black hole solution the natural variables one should use are the dual Plebański variables ($P_{\mu\nu}$), and if one wants to find an exact magnetically charged one the natural variables one should use are the standard Maxwell variables ($F_{\mu\nu}$). Therefore, it is not possible to have an exact solution with both charges with the same variables.

Yajima *et al.* [23] were the first to find electrically/magnetically charged black holes solutions to the EEH theory.

On the one hand Ruffini *et al.* [24] obtained a similar electrically charged solution, but they are devoted to study QED effects near the horizon and QED corrections to thermodynamical quantities as the black hole entropy, total energy, and maximally extractable energy. On the other hand, we analyze all the possible trajectories in the space-time of the electrically charged EEH black hole and study the vacuum polarization effects on its shadow, by using the Plebański dual variables. The constitutive equations (13) relate both the standard and the dual variables.

For the electrically charged case we assume the following ansatz for the electromagnetic field:

$$P_{\mu\nu} = \frac{Q}{r^2} (\delta_{\mu}^0 \delta_{\nu}^1 - \delta_{\mu}^1 \delta_{\nu}^0). \quad (15)$$

This ansatz satisfies the electromagnetic equation (9). The invariants, Eq. (6), read

$$s = \frac{Q^2}{2r^4}, \quad t = 0, \quad (16)$$

the pseudoinvariant t is $\mathbf{D} \cdot \mathbf{H}$.

Therefore, integrating the Einstein equations, the electrically charged static black hole solution reads

$$m(r) = M - \frac{\tilde{Q}^2}{2r}, \quad (17)$$

where the black hole charge is screened due to the Euler-Heisenberg vacuum polarization effect,

$$Q \rightarrow \tilde{Q} = Q \left(1 - \frac{\alpha}{225\pi} E_Q^2(r) \right)^{1/2}. \quad (18)$$

When the electric field $E_Q(r) \equiv \frac{Q}{r^2 E_c}$ of the charged black hole is overcritical, electron-positron pair productions take place, and E_Q is screened down to its critical value $E_c \equiv \frac{m^2 c^3}{e\hbar}$.

We use the units with $\hbar = c = 1$ throughout the article. We consider the electric field E_Q as a constant field at a given r [24]. Notice that Eq. (17) behaves asymptotically ($r \rightarrow \infty$) as the Reissner-Nordström (RN) solution. Additionally, for $\alpha = 0$, we recover the linear RN solution. For $Q = 0$ it reduces to the Schwarzschild solution.

A. The event horizon

The zeroes of the function $f(r)$ indicate the existence of a coordinates singularity which can eventually be removed by a suitable change of coordinates, like Eddington-Finkelstein ones. Thus, the event horizon locus r_h is determined by the condition $f(r_h) = 0$, which leads to

$$\frac{m(r_h)}{r_h} = \frac{1}{2}, \Rightarrow \frac{M}{r_h} - \frac{Q^2}{2r_h^2} \left(1 - \frac{\alpha}{225\pi} E_{Q_h}^2 \right) = \frac{1}{2}, \quad (19)$$

TABLE I. The comparison between the EEH event horizon locus $r_{EH_+} = r_{h_+}$ of Eq. (20) and that of the RN one r_{RN_+} when varying Q with fixed $M = 10^6 M_\odot$. We also show the screened charge of the black hole \tilde{Q} at the event horizon. The difference is visible in the last two digits.

Q/M	r_{RN_+}/M	\tilde{Q}/M	r_{EH_+}/M
0.4	1.916515139	0.39999991	1.916515177
0.5	1.86602540	0.49999998	1.86602551
0.6	1.8	0.59999996	1.80000039
0.7	1.7141428	0.69999993	1.7141436
0.8	1.6	0.7999999	1.600002
0.9	1.43589	0.8999997	1.43590
1	1.0	0.99998	1.0061

when using Eq. (17). Here $E_{Q_h} = E_Q(r_{RN_h})$ is the value of the electric field at the RN event horizon, since we are studying the QED Euler-Heisenberg correction to the RN black hole event horizon [24]. Solving this condition one obtains

$$r_{h_\pm} = M \pm \sqrt{M^2 - Q^2 \left(1 - \frac{\alpha}{225\pi} E_{Q_\pm}^2\right)}, \quad (20)$$

where $E_{Q_\pm} = E_Q(r_{RN_\pm})$, with the RN horizon locus $r_{RN_\pm} = M \pm \sqrt{M^2 - Q^2}$.

Due to the QED charge screening, the EEH event horizon barely stretches in comparison to the RN event horizon, as shown on Table I. On the other hand, the EEH inner horizon shrinks as shown on Table II.

1. The extreme case

In the extreme case, $r_{h_+} = r_{h_-} = r_{he}$. This happens when

$$r_{he}^2 = M^2 = Q^2 \left(1 - \frac{\alpha}{225\pi} E_{Q_{he}}^2\right). \quad (21)$$

Or, since $E_{Q_{he}} = E_Q(r_{RN_{he}} = Q = M) = \frac{Q}{M^2 E_c}$, one gets

TABLE II. The comparison between the EEH inner horizon locus $r_{EH_-} = r_{h_-}$ of Eq. (20) and that of the RN one r_{RN_-} when varying Q with fixed $M = 10^6 M_\odot$. We also show the screened charge of the black hole \tilde{Q} at the inner horizon. The difference is visible in the last two digits.

Q/M	r_{RN_-}/M	\tilde{Q}/M	r_{EH_-}/M
0.4	0.083	0.375	0.073
0.5	0.134	0.493	0.130
0.6	0.2	0.5975	0.198
0.7	0.2859	0.6991	0.2849
0.8	0.4	0.7996	0.3995
0.9	0.5641	0.8999	0.5638
1	1.0	0.99998	0.9939

$$r_{he} = M = |Q| \sqrt{1 - \frac{\alpha}{225\pi Q^2 E_c^2}}. \quad (22)$$

Due to the nonlinear term, when the charge Q is fixed, the extreme horizon shrinks compared to the RN case. The reason is that the charge screening effect decreases the electrostatic energy; hence, this leads to a smaller mass M for the extreme black hole [24], since $Q > M$.

IV. TRAJECTORIES OF TEST PARTICLES

In this section we study all possible trajectories of test particles on the equatorial plane ($\theta = \pi/2$) of the electrically charged Einstein-Euler-Heisenberg static black hole. Due to the spherical symmetry we can consider only these orbits without loss of generality [25]. We study the geodesic equations for uncharged and charged test particles, and also for photons. The problem reduces to analyze ordinary effective potentials. The test particles have at least two conserved quantities, corresponding to the two Killing vectors ∂_t , and ∂_ϕ , which correspond to the energy E and angular momentum l of the test particle.

A. Uncharged test particles

The geodesic equation for uncharged test particles reads

$$\frac{d^2 x^\mu}{d\tau^2} + \Gamma_{\sigma\rho}^\mu \frac{dx^\sigma}{d\tau} \frac{dx^\rho}{d\tau} = 0. \quad (23)$$

On the equatorial plane, the Lagrangian is given by

$$\mathcal{L} = -f(r)\dot{t}^2 + \frac{\dot{r}^2}{f(r)} + \frac{l^2}{r^2}. \quad (24)$$

Massive test particles travel on timelike geodesics $\mathcal{L} = -1$, while massless particles travel along null geodesics $\mathcal{L} = 0$. The two conserved quantities, namely the energy and the angular momentum are given by

$$E = f(r)\dot{t}, \quad l = r^2\dot{\phi}. \quad (25)$$

The components of the geodesic equation read

$$\begin{aligned} \ddot{t} &= -\frac{f'(r)}{f(r)} \dot{r} \dot{t}, \\ \ddot{r} &= -\frac{1}{2} f(r) f'(r) \dot{t}^2 + \frac{f'(r)}{2f(r)} \dot{r}^2 + r f(r) \dot{\phi}^2, \\ \ddot{\phi} &= -2l \frac{\dot{r}}{r^3}. \end{aligned} \quad (26)$$

Replacing the conserved quantities we obtain a first integration of the equation for the r component. We obtain an energylike equation $\dot{r}^2 + V_{\text{eff}}(r) = E^2$, where the effective potential reads

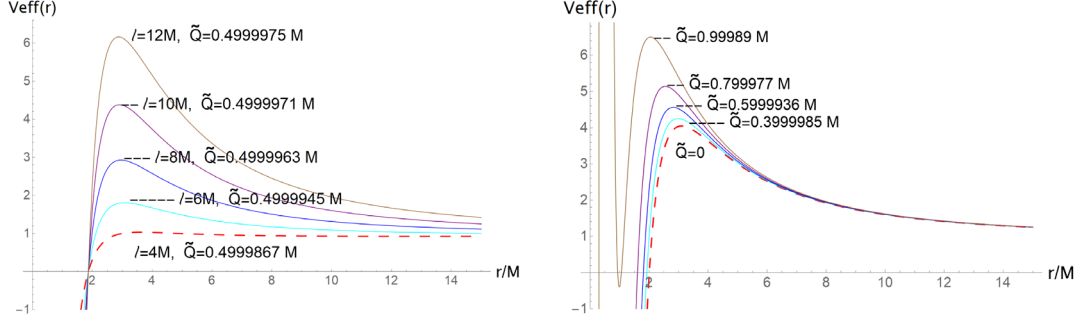


FIG. 1. The behavior of the EEH effective potential $V_{\text{eff}}(r)$ for massive test particles $\mathcal{L} = -1$ and fixed black hole mass $M = 10^5 M_{\odot}$ is shown. On the left-hand side we vary the angular momentum l with fixed RN charge $Q = 0.5M$. The dashed curve corresponds to a value of $l = 4M$, while each upper curve corresponds to bigger values of the angular momentum: $l/M = \{4, 6, 8, 10, 12\}$. On the right-hand side we vary the RN charge Q for fixed $l = 10M$. As the value of Q increases, the effective potential grows. The dashed curve corresponds to Schwarzschild, $Q = 0$. The RN charge values are $Q/M = \{0, 0.4, 0.6, 0.8, 1\}$. For each value of Q at a radius r there is a screened charge $\tilde{Q}(r)$. The values of the screened charge at the respective maximum locus $\tilde{Q}(r_n)$ are displayed on each plot; the nonlinear effects are barely visible. The maximum radius r_n depends on both l and \tilde{Q} , as it is shown later in Eq. (29).

$$V_{\text{eff}} = f(r) \left(\frac{l^2}{r^2} - \mathcal{L} \right). \quad (27)$$

$$E^2 - V_{\text{eff}}(r_n) = 0 \Rightarrow (1 - E^2)r_n^4 - 2Mr_n^3 + (l^2 + \tilde{Q}^2)r_n^2 + 2Ml^2r_n + \tilde{Q}^2l^2 = 0, \quad (28)$$

Figure 1 shows the behavior of the effective potential varying the angular momentum and the black hole charge. There exist maxima of the potential for values of l/M greater than 4. These correspond to unstable circular orbits of radius r_c as shown later in Fig. 3. For $l = 4M$ we find minima of the potential which correspond to stable circular orbits of radius r_s . Bound orbits may occur due to the existence of these minima. Figure 2 shows the behavior of the effective potential as varying the mass M of the black hole. These plots correspond to massive particles $\mathcal{L} = -1$.

In order that the massive particle $\mathcal{L} = -1$ remains in a circular orbit with constant $r = r_n$ the conditions to be fulfilled are $\dot{r} = 0$ and $\ddot{r} = 0$. Respectively,

$$V'_{\text{eff}}(r_n) = 0 \Rightarrow r_n^3 - \frac{l^2 + \tilde{Q}^2}{M}r_n^2 + 3l^2r_n - \frac{2\tilde{Q}^2l^2}{M} = 0, \quad (29)$$

where \tilde{Q} is the screened charge, Eq. (18), and r_n is one of the roots of the third degree polynomial of Eq. (29). From Eqs. (28), (29),

$$l^2 = \frac{r_n^2(Mr_n - \tilde{Q}^2)}{r_n^2 - 3Mr_n + 2\tilde{Q}^2}, \quad (30)$$

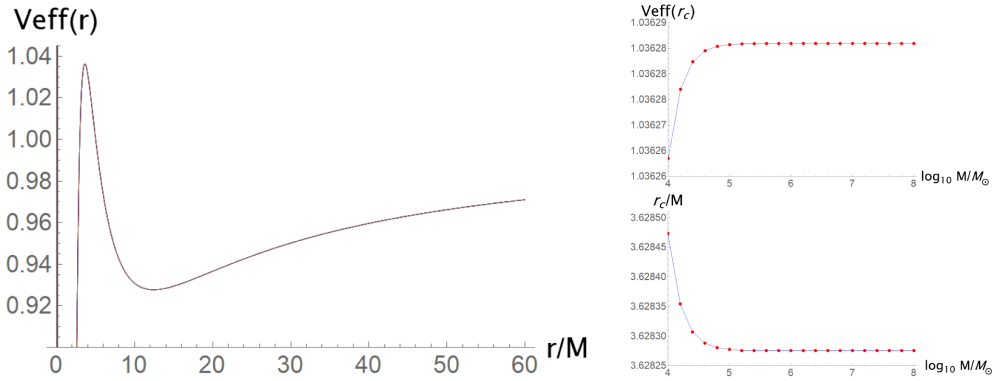


FIG. 2. The behavior of the EEH effective potential $V_{\text{eff}}(r)$ varying M for massive test particles $\mathcal{L} = -1$. The parameters are $l = 4M$, $Q = 0.5M$ and $M/M_{\odot} = \{10^5, 10^6, 10^7, 10^8\}$. As the solution is asymptotically RN, the nonlinear effects are barely visible, when increasing M on the left-hand side (lhs). Bound orbits are found for these values of the parameters. On the right-hand side (rhs) the mass M of the black hole varies from $M = 10^4 M_{\odot}$ to $M = 10^8 M_{\odot}$ in $10^{1/5} M_{\odot}$ steps. The maximum locus r_c (rhs down) barely decreases, and the effective potential evaluated on it $V_{\text{eff}}(r_c)$ (rhs up) barely increases as M increases. There seems to be an asymptote as $M \rightarrow \infty$ which would be analogue to the RN case $\alpha = 0$. The RN charge $Q = 0.5M$ is being screened for each value of r . For example, at $r = r_c$ for $M = 10^4 M_{\odot}$, the screened charge is $\tilde{Q} \approx 0.499867M$. Therefore, the differences between the EEH case when compared with the RN one are quantitatively very small.

TABLE III. We display the screened charge of the black hole \tilde{Q} at the ISCO, the EEH ISCO radius $r_{i\text{EH}} = r_i$, Eq. (32), with its corresponding angular momentum $l_{i\text{EH}} = l_i$, Eq. (30), and that of the RN case $r_{i\text{RN}}$ with $l_{i\text{RN}}$, when varying Q with fixed $M = 10^4 M_\odot$. The difference is visible in the last two digits.

Q/M	$l_{i\text{RN}}/M$	$r_{i\text{RN}}/M$	\tilde{Q}/M	$l_{i\text{EH}}/M$	$r_{i\text{EH}}/M$
0	$\sqrt{12}$	6	0	$\sqrt{12}$	6
0.4	3.3847209	5.752780	0.399989	3.3847253	5.752794
0.5	3.337737	5.606643	0.499977	3.337750	5.606682
0.6	3.277653	5.41984	0.599954	3.277684	5.41994
0.7	3.202220	5.18523	0.699912	3.202294	5.18546
0.8	3.10779	4.8908	0.79983	3.10797	4.8913
0.9	2.9879	4.5137	0.89968	2.9883	4.5151
1	2.8284	4	0.99928	2.8298	4.0045

$$E^2 = \frac{(r_n^2 - 2Mr_n + \tilde{Q}^2)^2}{r_n^2(r_n^2 - 3Mr_n + 2\tilde{Q}^2)}. \quad (31)$$

An analytic solution of Eq. (29) reads [26]

$$\frac{r_n}{M} = \mathcal{R} + 2\sqrt{\mathcal{D}} \cos\left(\frac{1}{3} \arccos \mathcal{B} + \frac{2}{3} n\pi\right), \quad n = 0, 1, 2. \quad (32)$$

The label n denotes each of the roots of the third degree polynomial. The solution $n = 0$ usually coincides with the locus r_s of a stable circular orbit, while the solution $n = 2$ usually coincides with that of an unstable circular orbit (UCO) r_c . The quantities,

$$\begin{aligned} \mathcal{R} &= \frac{l^2 + \tilde{Q}^2}{3M^2}, & \mathcal{D} &= \mathcal{R}^2 - \frac{l^2}{M^2}, \\ \mathcal{B} &= \left[\mathcal{R}^3 - \frac{l^2}{2M^4} (l^2 - \tilde{Q}^2) \right] \mathcal{D}^{-3/2}. \end{aligned} \quad (33)$$

The screened charge at the stable circular orbit is evaluated at the Reissner-Nordström stable circular orbit locus $r_{s\text{RN}}$, which corresponds to Eq. (32) for Q instead of \tilde{Q} . Analogously, for the UCO, the screened charge is $\tilde{Q}(r_{c\text{RN}})$.

1. Innermost stable circular orbit

When solving the cubic equation, Eq. (29), by the Cardano method [26] we find out that the discriminant $\Delta = \sqrt{\mathcal{D}^3(\mathcal{B}^2 - 1)}$ of the cubic vanishes when $\mathcal{B}^2 = 1$. This corresponds to the innermost stable circular orbit (ISCO),

and it depends on the parameters \tilde{Q}/M and l/M , as seen from Eq. (33). Thus, for a fixed \tilde{Q} we may compute the value of the angular momentum l_i which satisfies the condition $\mathcal{B}^2 = 1$, in order that the root of the Eq. (29) now corresponds to the radius r_i of the ISCO of the black hole with an electric charge \tilde{Q} at r_i .

In Table III we show the corresponding angular momentum l_i and ISCO radius r_i for the EEH black hole, when varying Q , in comparison with the RN case. The screened charge is now evaluated at the RN ISCO, $\tilde{Q}(r_{i\text{RN}})$. Due to the EH nonlinear contribution the ISCO barely stretches.

The ISCO satisfies the extremal condition [25],

$$\begin{aligned} V''_{\text{eff}}(r_i) = 0 &\Rightarrow 2Mr_i^3 - 3\tilde{Q}^2 r_i^2 \\ &- l_i^2(3r_i^2 - 12Mr_i + 10\tilde{Q}^2) = 0, \end{aligned} \quad (34)$$

which together with Eq. (30) for $r_s = r_i$ and $l = l_i$, gives

$$r_i^3 - 6Mr_i^2 + 9\tilde{Q}^2 r_i - 4\tilde{Q}^4/M = 0. \quad (35)$$

For the extreme case, Eq. (22),

$$l_{\text{ex}} = 2\sqrt{2}M = 2\sqrt{2}\tilde{Q}, \quad r_{i\text{ex}} = 4M = 4\tilde{Q}. \quad (36)$$

Although the ISCO stretches due to the EH nonlinear contribution when compared to the RN case, in the extreme case $r_{i\text{ex}} = 4\tilde{Q} < 4Q$, since $Q > M$.

In order to perform a second integration of the r component of the geodesic equation, Eq. (26), one should use the change of variable $u = 1/r$. From Eq. (27) with $\mathcal{L} = -1$, the integral to be solved reads

$$\pm\phi = \int \frac{du}{\sqrt{[E^2 - 1 + 2Mu]/l^2 - (1 + \tilde{Q}^2/l^2)u^2 + 2Mu^3 - \tilde{Q}^2 u^4}}. \quad (37)$$

Two points where the polynomial inside the square root vanishes correspond to the root of Eq. (29), i.e., the stable circular orbit for instance, $u_s = 1/r_s$. Then Eq. (37) becomes

$$\pm\phi = \int \frac{du}{(u - u_s)\sqrt{-\tilde{Q}^2 u^2 + 2(M - \tilde{Q}^2 u_s)u + u_s(M - \tilde{Q}^2 u_s - M/(l^2 u_s^2))}}. \quad (38)$$

Using the change of variable $\xi = (u - u_s)^{-1}$,

$$\mp\phi = \int \frac{d\xi}{\xi\sqrt{-\tilde{Q}^2 + \beta\xi + \delta\xi^2}}, \quad (39)$$

with $\beta = 2(M - 2\tilde{Q}^2 u_s)$ and $\delta = u_s(3M - 4\tilde{Q}^2 u_s - M^2/(l^2 u_s^2))$. The solution reads [27]

$$\mp\phi = \frac{1}{\sqrt{\delta}} \ln \left[2\sqrt{\delta(-\tilde{Q}^2 + \beta\xi + \delta\xi^2)} + 2\delta\xi + \beta \right], \quad \delta > 0, \quad \mp\phi = -\frac{1}{\sqrt{-\delta}} \arcsin \left[\frac{2\delta\xi + \beta}{\sqrt{4\delta\tilde{Q}^2 + \beta^2}} \right], \quad \delta < 0. \quad (40)$$

Figure 3 shows the trajectories of massive particles in the spacetime of EEH charged black hole.

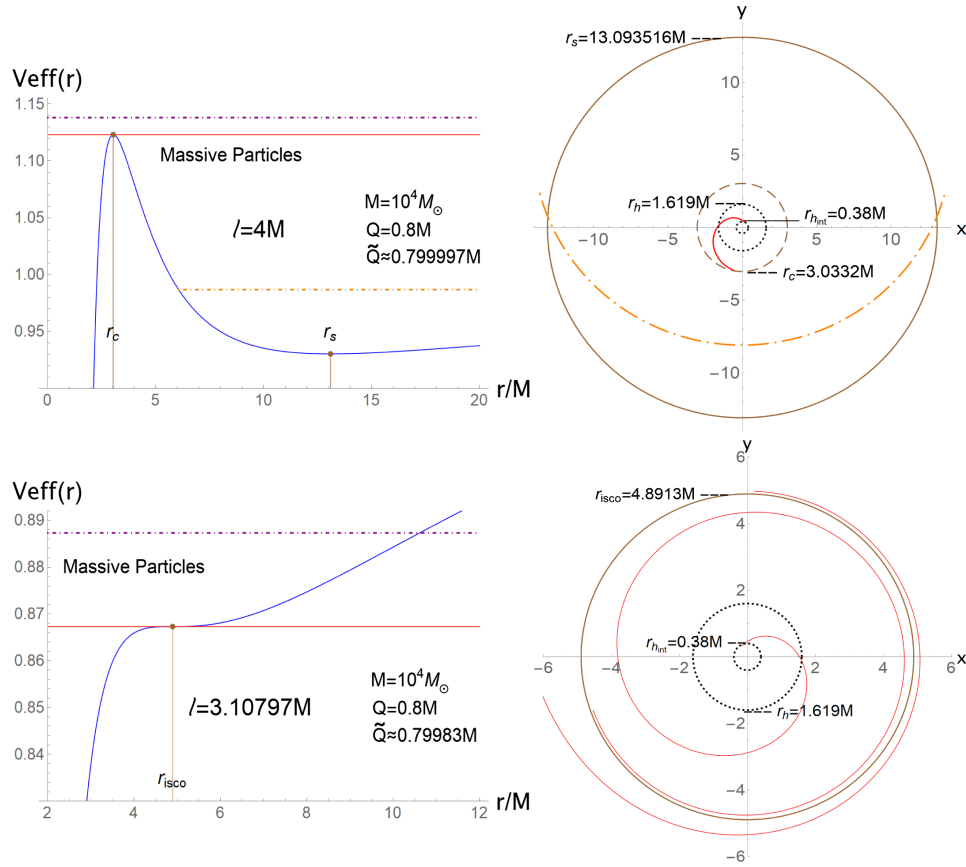


FIG. 3. The behavior of the EEH effective potential $V_{\text{eff}}(r)$ varying the angular momentum l for massive test particles $\mathcal{L} = -1$ with RN charge $Q = 0.8M$ and fixed black hole mass $M = 10^4 M_\odot$ (lhs), and the corresponding trajectories (rhs) are displayed. On the rhs the continuous circle corresponds to a stable circular orbit and the dashed circle corresponds to the unstable circular orbit (UCO), i.e., the solutions in Eq. (32). The dotted circles are the outer and the inner event horizons, Eq. (20), at $r_h = 1.619M$ and $r_{h_{\text{int}}} = 0.38M$ respectively. The dot-dashed line is the trajectory of a massive particle which goes near the black hole and returns to infinity. Finally, the continuous line corresponds to the trajectory of a particle that reaches the UCO and then falls into the black hole interior. It corresponds to the solution, Eq. (40). On the upper side we plot the case $l = 4M$, where there are both a stable and an unstable circular orbits. The plot below corresponds to the ISCO case with $l = 3.10797M$. We also show the screened charge \tilde{Q} at the ISCO (see Table III for \tilde{Q} at the ISCO).

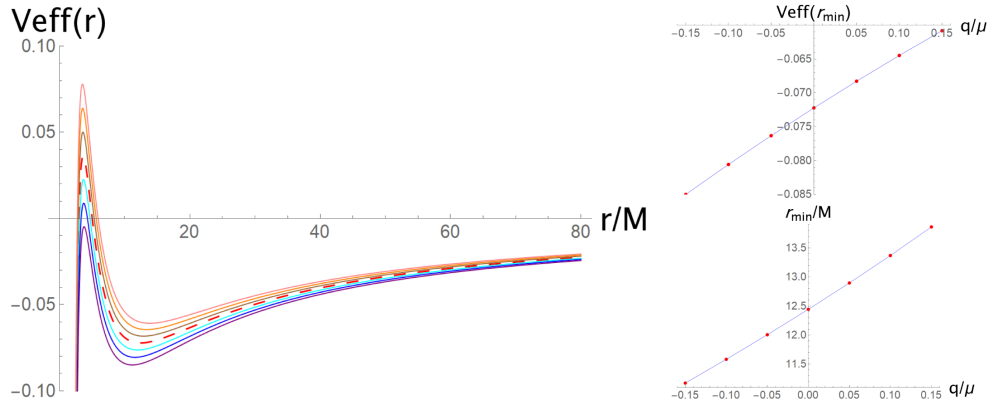


FIG. 4. The behavior of the EEH effective potential $V_{\text{eff}}(r)$ varying the test particle charge q/μ . The parameters are $l = 4M$, $\mathcal{E} = 1$, $M = 10^4 M_{\odot}$, $Q = 0.5M$ and $q/\mu = \{0, -0.05, -0.1, -0.15, 0.05, 0.1, 0.15\}$. The central dashed line corresponds to the uncharged test particle $q = 0$. The upper curves correspond to positive test charges and the lower ones correspond to negative test charges. On the lhs the effective potential is plotted and bound orbits are found. As in Fig. 2, the RN charge $Q = 0.5M$ is screened to $\tilde{Q} \approx 0.499867M$ at the maximum locus, now the test particle charge q is also screened. On the rhs we show the behavior of both the minimum locus r_{min} (rhs down) and the effective potential evaluated on it $V_{\text{eff}}(r_{\text{min}})$ (rhs up) while varying q/μ .

B. Charged test particles

The geodesic equation of a test particle with charge q and mass μ includes the contribution of the Lorentz force,

$$\frac{d^2 x^\alpha}{d\tau^2} + \Gamma_{\beta\delta}^\alpha \frac{dx^\beta}{d\tau} \frac{dx^\delta}{d\tau} = -\frac{q}{\mu} F^\alpha{}_\nu \frac{dx^\nu}{d\tau}. \quad (41)$$

For the electrically charged EEH black hole, by using the material equations, Eq. (13), it reads [1]

$$\frac{d^2 x^\alpha}{d\tau^2} + \Gamma_{\beta\delta}^\alpha \frac{dx^\beta}{d\tau} \frac{dx^\delta}{d\tau} = -\frac{q}{\mu} \left(1 - \frac{10\alpha}{225\pi} E_Q^2\right) P^\alpha{}_\nu \frac{dx^\nu}{d\tau}. \quad (42)$$

The Lagrangian, from which this geodesic equation arises, is given by [25]

$$\mathcal{L} = \left[-f(r)\dot{t}^2 + \frac{\dot{r}^2}{f(r)} + r^2\dot{\phi}^2\right] - \frac{2\tilde{q}\tilde{Q}}{\mu r}\dot{t}, \quad (43)$$

where due to the Euler-Heisenberg vacuum polarization effect the charge of the test particle is also screened,

$$q \rightarrow \tilde{q} = q \left(1 - \frac{19\alpha}{225\pi} E_Q^2\right)^{1/2}, \quad (44)$$

analogously to Eq. (18). The angular momentum is still $l = r^2\dot{\phi}$. From the t component of the geodesic equation we find the conserved quantity related to the energy of the charged test particle,

$$\mathcal{E} = f(r)\dot{t} + \frac{\tilde{q}\tilde{Q}}{\mu r}. \quad (45)$$

In the RN limit, $\alpha = 0$, we recover the usual expression for the energy of charged test particles, which involves the Coulomb potential. In the EH nonlinear case we get the Coulomb potential for the screened charges \tilde{Q} and \tilde{q} . When

the test particle is uncharged $q = 0$, the energies from Eq. (25) and Eq. (45) coincide, i.e., $\mathcal{E} = E$, as expected.

The components of the geodesic equation for charged test particles read

$$\begin{aligned} \ddot{t} + \frac{f'(r)}{f(r)} \dot{r} \dot{t} &= \frac{\dot{r}}{f(r)} \frac{\tilde{q}\tilde{Q}}{\mu r^2}, \\ \ddot{r} + \frac{1}{2} f(r) f'(r) \dot{t}^2 - \frac{f'(r)}{2f(r)} \dot{r}^2 - r f(r) \dot{\phi}^2 &= \frac{\tilde{q}\tilde{Q}}{\mu r^2} f(r) \dot{t}, \\ \ddot{\phi} + 2l \frac{\dot{r}}{r^3} &= 0. \end{aligned} \quad (46)$$

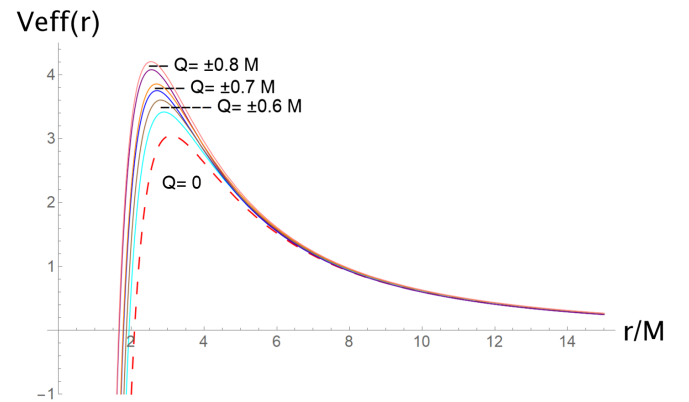


FIG. 5. The behavior of the EEH effective potential $V_{\text{eff}}(r)$ varying the RN charge Q . The dashed curve corresponds to Schwarzschild. The parameters are $l = 10M$, $\mathcal{E} = 1$, $q/\mu = 0.1$, $M = 10^5 M_{\odot}$, and $Q/M = \{0, -0.6, -0.7, -0.8, 0.6, 0.7, 0.8\}$. For bigger values of $|Q|$ the potential grows, but there is an upper curve and a lower one for each sign of the charge. For each value of Q at a radius r the charge $\tilde{Q}(r)$ is screened, as on the rhs of Fig. 1, also the particle charge $\tilde{q}(r)$ is screened.

After a first integration of the r component, we get an equation of the form $\dot{r}^2 + V_{\text{eff}}(r) = 0$, with the effective potential,

$$V_{\text{eff}} = f(r) \left(\frac{l^2}{r^2} + 1 \right) - \left[\mathcal{E} - \frac{\tilde{q} \tilde{Q}}{\mu r} \right]^2. \quad (47)$$

The effective potential depends on the energy \mathcal{E} , angular momentum l , and charge \tilde{q} of the test particle. We are interested in the product of the charges $\tilde{q} \tilde{Q}$. When both the black hole and the test particle have the same charge sign, the effective potential will grow due to an acting repulsive force. When the signs of the charges are opposite, there will be an attractive force.

This effect is shown in Fig. 4, where the maximum of the potential grows or decreases depending on the sign of both the black hole and the test particle charges. Nevertheless, the effect is small since we are considering test charges. In Fig. 5 we show the effect of varying the RN charge Q , considering both positive and negative charges, since the cross term of Eq. (47) depends lineally on the black hole charge. We may find maxima and minima of the potential, which would correspond to the critical radius of the unstable and of the stable circular orbits.

In order to perform a second integration of the r component, Eq. (47), we use the change of variable $u = 1/r$. The integral to be solved reads

$$\pm\phi = \int \frac{du}{\sqrt{[\mathcal{E}^2 - 1 + 2(M - \mathcal{E}\tilde{Q}\tilde{q}/\mu)u]/l^2 - [1 + \tilde{Q}^2/l^2 - \tilde{q}^2\tilde{Q}^2/(\mu^2 l^2)]u^2 + 2Mu^3 - \tilde{Q}^2u^4}}. \quad (48)$$

Analogously, the polynomial inside the square root vanishes at the critical points u_{ch} . Hence, Eq. (48) becomes

$$\pm\phi = \int \frac{du}{(u - u_{ch}) \sqrt{-\tilde{Q}^2u^2 + 2(M - \tilde{Q}^2u_{ch})u + u_{ch}(M - \tilde{Q}^2u_{ch} - (M - \mathcal{E}\tilde{Q}\tilde{q}/\mu)/(l^2u_{ch}^2))}}. \quad (49)$$

Using the change of variable $\xi = (u - u_{ch})^{-1}$, the integral to be solved is equivalent to that of Eq. (39), with $\beta = 2(M - 2\tilde{Q}^2u_{ch})$ and $\delta = u_{ch}(3M - 4\tilde{Q}^2u_{ch} - (M - \mathcal{E}\tilde{Q}\tilde{q}/\mu)/(l^2u_{ch}^2))$. The solution is Eq. (40) with the corresponding values of β and δ .

C. Massless test particles

The effective potential for massless test particles (like gravitons) is that of Eq. (27) with $\mathcal{L} = 0$, i.e.,

$$V_{\text{eff}} = f(r) \frac{l^2}{r^2}. \quad (50)$$

In order that the massless particle remains in a circular orbit with $r = r_{c_g} = \text{const}$ the conditions to be fulfilled, are

$$\dot{r} = 0 \Rightarrow E^2 - V_{\text{eff}}(r_{c_g}) = 0, \quad \ddot{r} = 0 \Rightarrow V'_{\text{eff}}(r_{c_g}) = 0. \quad (51)$$

From $E^2 - V_{\text{eff}}(r_{c_g}) = 0$ one has

$$\eta^2 = \frac{r_{c_g}^2}{f(r_{c_g})}, \quad (52)$$

where $\eta \equiv \frac{l}{E}$ is the impact parameter and $r = r_{c_g}$ is one of the roots of the polynomial arising from the condition $V'_{\text{eff}}(r) = 0$, i.e.,

$$r(r - 3M) + 2\tilde{Q}^2 = 0. \quad (53)$$

Its solutions read

$$r_{c_{g\pm}} = \frac{3}{2}M \left(1 \pm \sqrt{1 - \frac{8}{9} \left(\frac{\tilde{Q}}{M} \right)^2} \right), \quad (54)$$

and $r_{c_g} = r_{c_{g+}}$ corresponds to the radius of the massless particles unstable circular orbit (UCO).

Analogously to the massive particles case, we use the change of variable $u = 1/r$ to perform a second integration. From Eq. (50), the integral to be solved reads

$$\begin{aligned} \pm\phi &= \int \frac{du}{\sqrt{-\tilde{Q}^2u^4 + 2Mu^3 - u^2 + \frac{1}{\eta^2}}}, \\ &= \int \frac{du}{(u - u_{c_g}) \sqrt{-\tilde{Q}^2u^2 + 2(M - \tilde{Q}^2u_{c_g})u + u_{c_g}(M - \tilde{Q}^2u_{c_g})}}. \end{aligned} \quad (55)$$

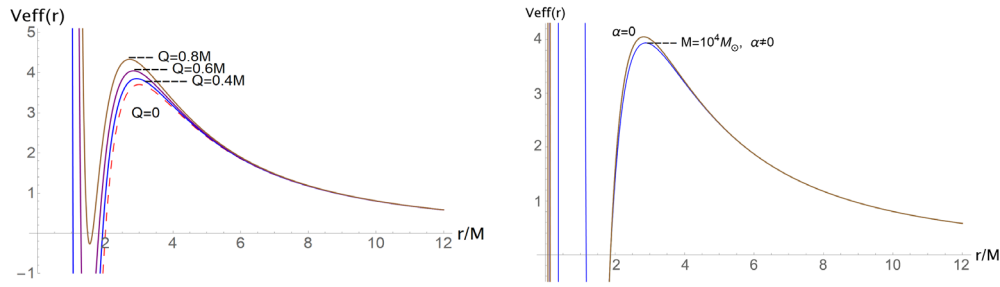


FIG. 6. On the lhs we show the effective potential for photons, Eq. (63), for different values of the RN charge Q . The values of the parameters are $l = 10M$, $M = 10^4 M_\odot$, and $Q/M = \{0, 0.4, 0.6, 0.8\}$. The dashed curve corresponds to Schwarzschild ($Q = 0$). As Q increases the potential grows, it is always located under the RN case, since Q is screened for each value of r . This is shown on the rhs, where we vary the mass M of the black hole, for fixed $l = 10M$ and $Q = 0.5M$. The cases $M/M_\odot = \{10^5, 10^6\}$ are together on the top of the plot with the linear case $\alpha = 0$, but the screening effect becomes relevant for $M = 10^4 M_\odot$ and near the maximum of the potential, which corresponds to the UCO. There are no stable bound orbits outside the event horizon.

In this case, the points where the polynomial inside the square root vanishes correspond to the UCO $u_{c_g} = 1/r_{c_g}$. Using the change of variable $\xi = (u - u_{c_g})^{-1}$, the integral to be solved is equivalent to that of Eq. (39), with $\beta = 2(M - 2\tilde{Q}^2 u_{c_g})$ and $\delta = u_{c_g}(3M - 4\tilde{Q}^2 u_{c_g})$, and the solution is Eq. (40).

D. Photons

In linear Maxwell-Lorentz electrodynamics, the discontinuities of the field propagate according to the equation for the characteristic surfaces, which in standard optics is known as eikonal equation. On a curved spacetime the equation for the characteristic surfaces reads

$$g^{\mu\nu} S_{,\mu} S_{,\nu} = 0, \quad (56)$$

the corresponding linear photons travel along null geodesics of the geometrical metric $g^{\mu\nu}$. In EH nonlinear electrodynamics, photons propagate along null geodesics of the effective Plebański pseudometric $\gamma^{\mu\nu}$ [1] given by

$$\gamma^{\mu\nu} = g^{\mu\nu} + \frac{64\pi\alpha^2}{45m^4} T^{\mu\nu}, \quad (57)$$

which differs from the geometrical metric $g^{\mu\nu}$, since it contains the energy-momentum tensor as well. Replacing the energy-momentum tensor, Eq. (11), with $t = 0$ and up to the leading order in α , one obtains

$$\gamma^{\mu\nu} = \left(1 + \frac{16\alpha^2}{45m^4} s\right) g^{\mu\nu} + \frac{16\alpha^2}{45m^4} P^{\mu\beta} P^\nu{}_\beta. \quad (58)$$

The propagation equation for the nonlinear electromagnetic field discontinuities reads

$$\gamma^{\mu\nu} S_{,\mu} S_{,\nu} = 0, \quad (59)$$

where $S_{,\mu}$ are the normal vectors to the characteristic surface S . For the EEH theory the propagation equation reads

$$\left[\left(1 + \frac{16\alpha^2}{45m^4} s\right) g^{\mu\nu} + \frac{16\alpha^2}{45m^4} P^{\mu\beta} P^\nu{}_\beta \right] S_{,\mu} S_{,\nu} = 0. \quad (60)$$

Therefore, the energy-momentum tensor, $T_{\mu\nu}$ of the EH nonlinear field is responsible for the fact that these surfaces are not null surfaces of the geometrical metric, obeying Eq. (56). However, for $\alpha = 0$, i.e., linear Maxwell-Lorentz electrodynamics, both metrics coincide.

Hence, the trajectories of nonlinear photons are obtained from the effective metric Eq. (57),

$$\gamma_{\mu\nu} \dot{x}^\mu \dot{x}^\nu = \left[g_{\mu\nu} - \frac{64\pi\alpha^2}{45m^4} T_{\mu\nu} \right] \dot{x}^\mu \dot{x}^\nu = 0. \quad (61)$$

On the equatorial plane, the trajectories for photons satisfy the equation,

$$\dot{r}^2 + \left[1 - \frac{32\alpha^2}{45m^4} s \right] f(r) r^2 \dot{\phi}^2 = (f(r) \dot{t})^2. \quad (62)$$

In order to compare it with the RN case, $\alpha = 0$, we introduce the constants of motion, Eq. (25). Identifying $\alpha = e^2/4\pi$ and $2s = E_Q^2 E_c^2$, the analogous effective potential for nonlinear photons reads

$$V_{\text{eff}} = \left(1 - \frac{20\alpha}{225\pi} E_Q^2 \right) \frac{f(r) l^2}{r^2}, \quad (63)$$

which differs from Eq. (50) by the factor $-20\alpha E_Q^2/225\pi$. Both potentials coincide in the linear case $\alpha = 0$.

On the left-hand side of Fig. 6 the effect on the effective potential of varying the RN charge Q is shown. It lays always under that of the linear RN case. On the right-hand side of Fig. 6 we show the effect of varying the mass M of the black hole. We observe that the effect is barely appreciable, for some values of the parameters one must consider the screening effect on the light trajectories.

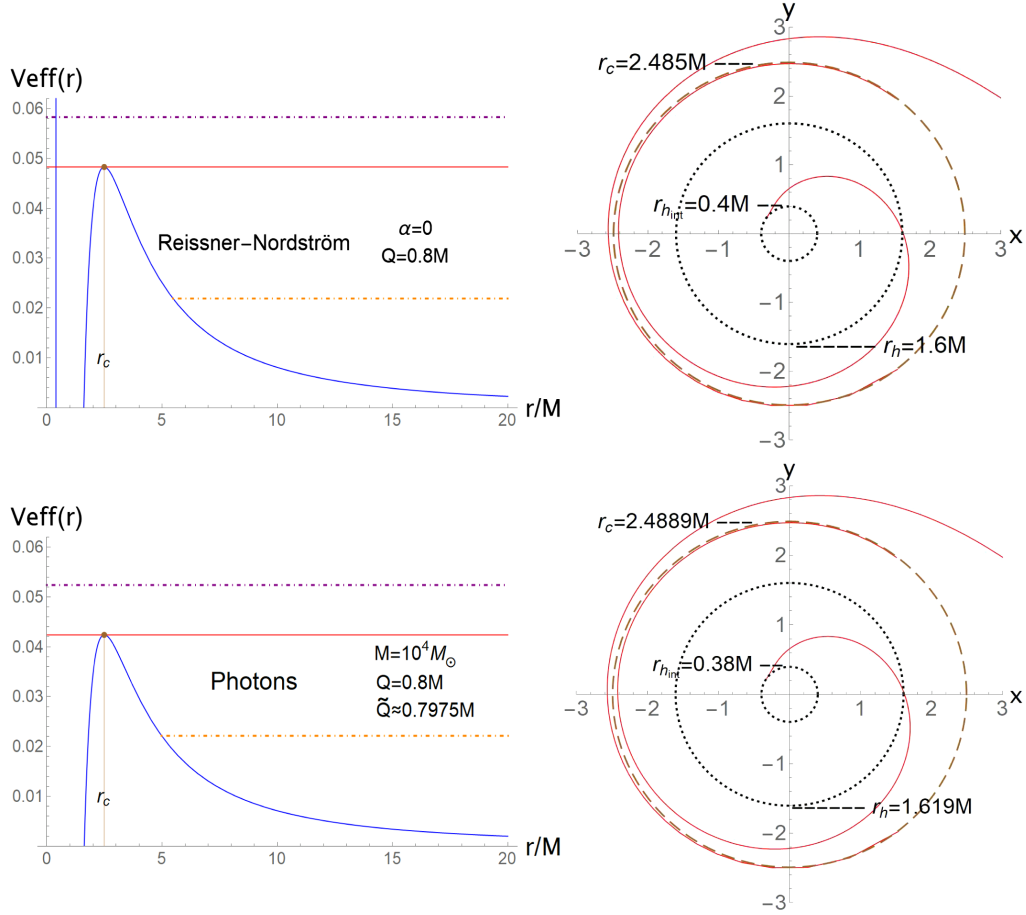


FIG. 7. The comparison between the effective potential for photons in the EEH black hole (down) and that in the linear RN one $\alpha = 0$ (up), with fixed mass $M = 10^4 M_\odot$ and RN charge $Q = 0.8M$. Since in the EEH case the charged is screened, we show its value at the UCO $\tilde{Q}(r_c)$. On the rhs of each potential we show the corresponding trajectories (continuous line) of a particle that reaches the UCO (dashed circles) and then falls into the event horizon and reaches the inner horizon (dotted circles). There are no minima of the potential; thus there are no stable bound orbits. The screening effect stretches the light ring when compared to the RN case.

On the other hand, the equations of motion on the equatorial plane are now

$$(\dot{t}, \dot{r}, \dot{\theta}, \dot{\phi}) = \left(\left[1 - \frac{10\alpha}{225\pi} E_Q^2 \right] \frac{E}{f(r)}, \left[1 - \frac{10\alpha}{225\pi} E_Q^2 \right] \sqrt{R(r)}, 0, \left[1 + \frac{10\alpha}{225\pi} E_Q^2 \right] \frac{l}{r^2} \right), \quad (64)$$

with the effective potential,

$$R(r) = E^2 - \left(1 + \frac{10\alpha}{225\pi} E_Q^2 \right) f(r) \frac{l^2}{r^2}. \quad (65)$$

Notice that the constants of motion E and l contain now an EH term.

The photons on the light ring satisfy the conditions $R(r_c) = 0$ and $R'(r_c) = 0$. The impact parameter η now reads

$$\eta^2 = \frac{r_c^2}{f(r_c)} \left(\frac{1 - \frac{10\alpha}{225\pi} E_Q^2}{1 + \frac{10\alpha}{225\pi} E_Q^2} \right). \quad (66)$$

Thus, from the second condition $R'(r_c) = 0 \Rightarrow V'_{\text{eff}}(r_c) = 0$, with $V_{\text{eff}}(r)$ the effective potential for massless particles, Eq. (50). This means that $r_c = r_{c_g}$, Eq. (54).

The second integration to be performed is, up to the leading term on α ,

$$\frac{\pm\phi}{1 + \frac{10\alpha}{225\pi} E_Q^2} = \int \frac{du}{\sqrt{-\tilde{Q}^2 u^4 + 2Mu^3 - u^2 + \frac{1}{\eta_Q^2}}}, \quad (67)$$

which is similar to that of Eq. (55) with $\eta_Q \approx \eta / [1 - \frac{10\alpha}{225\pi} E_Q^2]$ and η of Eq. (66). Hence, the solution is that of Eq. (40) with $\beta = 2(M - 2\tilde{Q}^2 u_c)$, $\delta = u_c(3M - 4\tilde{Q}^2 u_c)$, and considering the EH term dividing ϕ on Eq. (67). The critical point corresponds to the light ring $u_c = 1/r_c$.

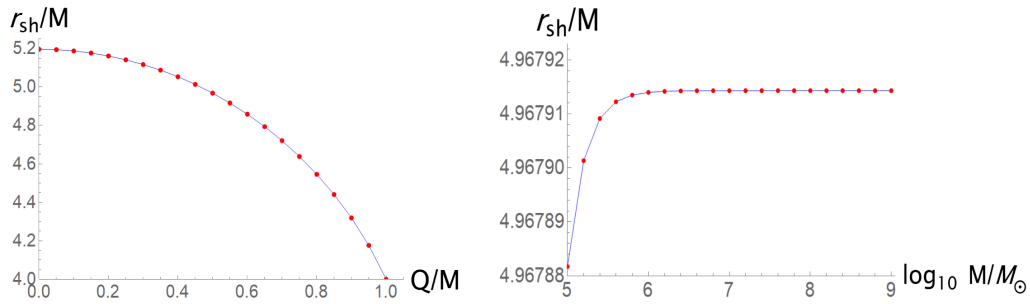


FIG. 8. EEH black hole shadow radius r_{sh} . On the lhs we vary the RN charge from $Q = 0$ to $Q = M$ in 0.05 steps, with fixed mass $M = 10^5 M_\odot$. As Q increases, the shadow shrinks. On the rhs we vary M from $M = 10^5 M_\odot$ to $M = 10^9 M_\odot$ in $10^{1/5} M_\odot$ increments, with fixed RN charge $Q = 0.5M$. As M increases, r_{sh} increases; nevertheless the EEH shadow is always inside of the RN one, which would correspond to the asymptote $M \rightarrow \infty$.

Figure 7 shows the comparison between the effective potential for photons in the RN case, and that in the EEH case. These potentials have no minimum; thus there cannot exist stable bound orbits as in the case for massive particles (see Fig. 3). There are unstable circular orbits at the maxima of the potential which correspond to the light rings.

V. SHADOW OF THE EINSTEIN-EULER-HEISENBERG BLACK HOLE

As it is well known, the spacetime curvature deflects the light trajectories. In particular the strong gravitational fields, like the ones generated by black holes, are able to increase the deflection angles significantly. In particular, they can produce unstable circular orbits of light around them, the so-called light rings. Since the orbits are not stable, part of the photons leaves them and gets out to a distant observer and the other part of them goes into the event horizon and falls down into the black hole interior. They are not a radiation source.

As it was already mentioned, in nonlinear electrodynamics, photons follow null geodesics of the effective Plebański pseudometric, which differ from the null geodesics of the geometrical metric followed by the massless particles like gravitons. In the case of photons the unstable circular orbits are the light rings, and the scattered photons reaching a distant observer are the boundary of the black hole shadow. Each point of the boundary is associated to a particular orbit [28].

Photons follow null geodesics of $\gamma^{\mu\nu}$, Eq. (58). From Eq. (64), the covariant momenta $p_\mu = \gamma_{\mu\nu} \dot{x}^\nu$ in the equatorial plane, up to first order in α , read

$$p_\mu = \left(-E, \frac{\sqrt{R(r)}}{f(r)}, 0, l \right), \quad (68)$$

with the function $R(r)$ given by Eq. (65). Now, we calculate the plane of the image for a distant observer in the equatorial plane with fixed coordinates $r = r_0$, $\theta = \pi/2$, and whose worldlines are perpendicular to the hypersurface $t = t_0 = \text{const}$. A basis of this frame is given by [21,29],

$$\begin{aligned} e_{(t)}^\mu &= \left(\frac{1}{\sqrt{f(r)}}, 0, 0, 0 \right), & e_{(r)}^\mu &= (0, \sqrt{f(r)}, 0, 0), \\ e_{(\theta)}^\mu &= \left(0, 0, \frac{1}{r}, 0 \right), & e_{(\phi)}^\mu &= \left(0, 0, 0, \frac{l}{r} \right). \end{aligned} \quad (69)$$

In this basis the momenta $\mathbf{p}^{(\alpha)} = \eta^{(\alpha\beta)} e_{(\beta)}^\mu p_\mu$ of the photon read

$$\mathbf{p}^{(\alpha)} = \left(\frac{E}{\sqrt{f(r)}}, \sqrt{\frac{R(r)}{f(r)}}, 0, \frac{l}{r} \right). \quad (70)$$

In terms of the impact parameter η , the celestial coordinates x and y , for $r_0 \rightarrow \infty$ and $\theta_0 = \pi/2$, are the following:

$$y = r_0 \left(\frac{\mathbf{p}^{(\theta)}}{\mathbf{p}^{(t)}} \right)_0 = 0, \quad x = -r_0 \left(\frac{\mathbf{p}^{(\phi)}}{\mathbf{p}^{(t)}} \right)_0 = -\eta. \quad (71)$$

If the observer is in the equatorial plane, the light ring only determines two points of the shadow boundary. Taking advantage of the spherical symmetry this result can be generalized for distant observers outside of the equatorial plane, by using Eq. (66).

Hence, the celestial coordinates fulfill the equation for the circle,

$$x^2 + y^2 = \left(\sqrt{\frac{1 - \frac{10\alpha}{225\pi} E_Q^2}{1 + \frac{10\alpha}{225\pi} E_Q^2}} \frac{r_c}{\sqrt{f(r_c)}} \right)^2. \quad (72)$$

We recover the linear Reissner-Nordström case for $\alpha = 0$. Equation (72) corresponds to the shadow of the EEH black hole. This result means that although the photons remain in a circle of radius r_c , the distant observer measures a ring which contains not only the factor $f(r_c)^{-1/2}$, but also a factor containing the EH nonlinear term. This factor is always less than 1. Hence, the EEH shadow is always inside of the RN one, $r_{sh\text{EEH}} < r_{sh\text{RN}}$.

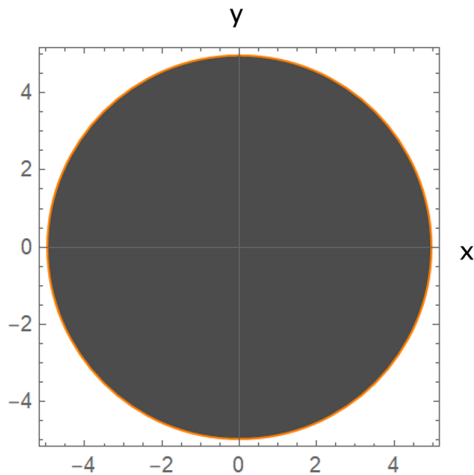


FIG. 9. EEH black hole shadow for fixed mass $M = 10^5 M_\odot$ and RN charge $Q = 0.5M$. The shadow of the static spherically symmetric EEH black hole is a circle which corresponds to Eq. (72). For $Q = 0.5M$ the RN shadow $r_{sh_{RN}} \approx 4.967914M$, the screened charge $\tilde{Q}(r_{sh_{RN}}) \approx 0.4999964M$ and the EEH shadow $r_{sh_{EH}} \approx 4.967882M$. The difference is visible in the last digits, and on the rhs of Fig. 8 we display it for different values of M .

For the extreme RN case $Q = M$ the shadow radius is $r_{sh_{RN}} = 4Q$, while for the extreme EEH case Eq. (22), the shadow radius is $r_{sh} = 4\tilde{Q} < 4Q$. We display the shadow radius in Fig. 8 varying the values of the RN charge Q/M and the mass M . In Fig. 9 we display the shadow of the EEH black hole for fixed Q/M and M .

VI. CONCLUSIONS AND SUMMARY

We consider the effective QED theory after one-loop, i.e., the Euler-Heisenberg nonlinear electrodynamics. The vacuum is treated as a specific type of medium, the polarizability properties of which are determined by the clouds of virtual charges surrounding the real ones, this represents a screening effect of the real charges. We found an Einstein-Euler-Heisenberg generalization of the Reissner-Nordström black hole solution. The Einstein-Euler-Heisenberg static black hole solution is asymptotically Reissner-Nordström and reduces to Reissner-Nordström for $\alpha = 0$. Moreover, for $Q = 0$ it

reduces to the Schwarzschild black hole. The screening effect on the charge stretches the size of the event horizon. In the extreme case of the Einstein-Euler-Heisenberg black hole, the horizon shrinks compared to the extreme RN horizon and the charge becomes greater than the mass.

We studied all the possible trajectories in this spacetime, by analytically integrating the geodesic equations and analyzing the corresponding effective potentials. The stable and the unstable circular orbits of massive test particles are barely modified due to the EH nonlinear contribution. In particular the ISCO barely stretches when compared to the RN one. We also studied the trajectories of charged test particles, considering the contribution of the Lorentz force. We find out that the test particle charge is also screened due to the vacuum polarization effect.

The screening effect on the trajectories of uncharged and charged test particles is barely visible. Nevertheless the effect becomes relevant for the photons trajectories, due to the fact that the effective Plebański pseudometric contains the energy-momentum tensor of the nonlinear Euler-Heisenberg electromagnetic field [1,30]. The effective potential for the nonlinear photons lays always under that for the linear Reissner-Nordström ones.

We also studied the shadow of the black hole measured by a distant observer, by means of the effective Plebański pseudometric. The shadow barely shrinks when we consider the Euler-Heisenberg screening effect. The Einstein-Euler-Heisenberg black hole shadow lays always inside the shadow of the RN black hole. It is worthwhile to stress the fact that the tiny variations of the shadow induced by the Einstein-Euler-Heisenberg metric (or the RN metric) are in general not observable, unless one has extremely accurate mass and distance measurements of the black hole, what is usually not the case. Notice that a Schwarzschild black hole with a slightly decreased mass could produce the exactly same shadow.

ACKNOWLEDGMENTS

This work was partially supported by “Programa Especial de Apoyo a la Investigación” of Universidad Autónoma Metropolitana, Ref. II3. D. Amaro acknowledges a fellowship from Universidad Autónoma Metropolitana.

- [1] J.F. Plebański, *Lectures on Nonlinear Electrodynamics* (Nordita, Copenhagen, 1970).
- [2] E. Ayón-Beato and A. García, Regular Black Hole in General Relativity Coupled to Nonlinear Electrodynamics, *Phys. Rev. Lett.* **80**, 5056 (1998).
- [3] G. Mie, Grundlagen einer Theorie der Materie, *Ann. Phys. (Leipzig)* **342**, 511 (1912).

- [4] M. Born and L. Infeld, Foundations of the new field theory, *Proc. R. Soc. A* **144**, 425 (1934).
- [5] B. Hoffmann, Gravitational and electromagnetic mass in the Born-Infeld electrodynamics, *Phys. Rev.* **47**, 877 (1935).
- [6] H. Salazar, A. Garcia, and J. Plebański, Duality rotations and type D solutions to Einstein equations with nonlinear

- electromagnetic sources, *J. Math. Phys. (N.Y.)* **28**, 2171 (1987).
- [7] A. Garcia, H. Salazar, and J. Plebański, Type-D solutions of the Einstein and Born-Infeld nonlinear-electrodynamics equations, II. *Nuovo Cimento* **84**, 65 (1984).
- [8] N. Bretón, Geodesic structure of the Born-Infeld black hole, *Classical Quantum Gravity* **19**, 601 (2002).
- [9] E. Fradkin and A. Tseytlin, Non-linear electrodynamics from quantized strings, *Phys. Lett.* **163B**, 123 (1985).
- [10] A. Tseytlin, Vector field effective action in the open superstring theory, *Nucl. Phys.* **B276**, 391 (1986); Erratum, *Nucl. Phys.* **B291**, 876 (1987).
- [11] R. G. Leigh, Dirac-Born-Infeld action from Dirichlet σ -model, *Mod. Phys. Lett. A* **04**, 2767 (1989).
- [12] L. de Fossé, P. Koerber, and A. Sevrin, The uniqueness of the Abelian Born-Infeld action, *Nucl. Phys.* **B603**, 413 (2001).
- [13] G. W. Gibbons, Born-Infeld particles and Dirichlet p-branes, *Nucl. Phys.* **B514**, 603 (1998).
- [14] W. Heisenberg and H. Euler, Folgerungen aus der Diracschen Theorie des Positrons, *Z. Phys.* **98**, 714 (1936).
- [15] S. Weinberg, *The Quantum Theory of Fields* (Cambridge University Press, Cambridge, England, 1995).
- [16] Yu. N. Obukhov and G. F. Rubilar, Fresnel analysis of the wave propagation in nonlinear Electrodynamics, *Phys. Rev. D* **66**, 024042 (2002).
- [17] G. Brodin, M. Marklund, and L. Stenflo, Proposal for Detection of QED Vacuum Nonlinearities in Maxwell's Equations by the Use of Waveguides, *Phys. Rev. Lett.* **87**, 171801 (2001).
- [18] G. Boillat, Nonlinear electrodynamics: Lagrangians and equations of motion, *J. Math. Phys. (N.Y.)* **11**, 941 (1970).
- [19] F. W. Hehl and Yu. N. Obukhov, *Foundations of Classical Electrodynamics* (Birkhäuser Boston, USA, 2003).
- [20] The Event Horizon Telescope Collaboration, First M87 event horizon telescope results. I. The shadow of the supermassive black hole, *Astrophys. J. Lett.* **875**, L1 (2019).
- [21] J. M. Bardeen, Timelike and null geodesics in the Kerr metric, in *Black Holes*, edited by C. DeWitt and B. S. DeWitt (Gordon and Breach, New York, 1973), p. 215.
- [22] G. W. Gibbons and C. A. R. Herdeiro, The Melvin universe in Born-Infeld theory and other theories of nonlinear electrodynamics, *Classical Quantum Gravity* **18**, 1677 (2001).
- [23] H. Yajima and T. Tamaki, Black hole solutions in Euler-Heisenberg theory, *Phys. Rev. D* **63**, 064007 (2001).
- [24] R. Ruffini, Y.-B. Wu, and S.-S. Xue, Einstein-Euler-Heisenberg theory and charged black holes, *Phys. Rev. D* **88**, 085004 (2013).
- [25] S. Chandrasekhar, *The Mathematical Theory of Black Holes* (Oxford University Press, New York, 1983).
- [26] R. W. D. Nickalls, A new approach to solving the cubic: Cardan's solution revealed, *Math. Gaz.* **77**, 354 (1993).
- [27] V. Enolski, E. Hackmann, V. Kagramanova, J. Kunz, and C. Lämmerzahl, Inversion of hyperelliptic integrals of arbitrary genus with application to particle motion in general relativity, *J. Geom. Phys.* **61**, 899 (2011).
- [28] V. P. Cunha and A. R. Herdeiro, Shadows and strong gravitational lensing: A brief review, *Gen. Relativ. Gravit.* **50**, 42 (2018).
- [29] J. M. Bardeen, W. H. Press, and S. Teukolsky, Rotating Black Holes: Locally nonrotating frames, energy extraction, and scalar synchrotron radiation, *Astrophys. J.* **178**, 347 (1972).
- [30] M. Novello, V. De Lorenci, J. Salim, and R. Klippert, Geometrical aspects of light propagation in nonlinear electrodynamics, *Phys. Rev. D* **61**, 045001 (2000).